https://doi.org/10.1016/j.nanoen.2021.106782

Engraved Pattern Spacer Triboelectric Nanogenerators for Mechanical Energy Harvesting

Wei Zhong, Bingang Xu*, Yuanyuan Gao

Research Institute of Intelligent Wearable Systems, Nanotechnology Center, Institute of Textiles and Clothing, The Hong Kong Polytechnic University, 999077, Hong Kong

* Corresponding author. E-mail address: tcxubg@polyu.edu.hk (B. Xu).

Abstract:

The emergence of triboelectric nanogenerators provides convenience for harvesting mechanical energy from the environment, and the contact-separation mode is one of the most basic operation modes of triboelectric nanogenerators. The preparation of the triboelectric nanogenerator of this mode usually requires the addition of third-party spacers or the overall deformation of its own substrate. Here, we propose an engraved patterned spacer triboelectric nanogenerator (EPS-TENG) to get rid of these unfavorable constraints. The spacers used by the EPS-TENG are made by engraving the substrate according to the designed and folded patterns. The engraved pattern spacers can be elastically deformed when subject to mechanical impact, and will automatically recover after the impact force is removed, which is perfectly adapted to external periodic mechanical impacts. The peak power of the device reached 92.34 μW, and 8.48 μW of average power could be achieved. The driving demonstration of the timer reveals that the EPS-TENG has great application prospects. The EPS-TENG with such excellent performance can not only contribute to the harvesting of mechanical energy in the environment, but also setting a useful reference for the research of engraved spacer triboelectric nanogenerators.

Keywords

triboelectric nanogenerator, contact-separation mode, engraved pattern spacer, semi-

ellipse, mechanical energy harvesting

Introduction

Since the advent of the triboelectric nanogenerator (TENG) in 2012,[1] it has immediately attracted people's attention and received a lot of exciting research. The TENG is rooted in Maxwell's displacement current, based on the coupling of triboelectric effect and electrostatic induction,[2] and is especially good at scavenging low-grade mechanical energy.[3, 4] Much work is devoted to the use of TENGs for energy harvesting, such as human motion,[5-10] water wave,[11-15] wind,[16-20] raindrop,[21-27] and vehicle vibration.[28-31] These widely distributed mechanical energy harvested from the environment can be used to power functional sensors to form self-powered sensing systems for common applications such as anti-theft,[32] respiration monitoring,[33] water quality monitoring,[34] temperature and humidity sensing,[35] voice recognition,[36] and tilt measurement.[37, 38]

Although various TENG devices have been developed, there are only four basic working modes, namely contact-separation mode, freestanding triboelectric-layer mode, lateral sliding mode, and single electrode mode.[2] Here, the contact-separation mode is the basis of our work. This mode relies on external impact to make the triboelectronegative material and the tribometal electrode contact each other. After the impact is eliminated, the two contact surfaces need to be separated by the elasticity of the spacer or the substrate to meet the next external impact. Obviously, in the contact-separation mode TENG, the separation between the triboelectronegative material and the tribometal electrode is very critical. There are two main methods for introducing this separation. One is to use additional spacers, such as gaskets,[39, 40] springs,[41] and sponge,[42] which will increase the cost of TENGs for design, manufacture and installation of spacers, and sometimes these spacers also lack flexibility.[43] The other requires the substrate itself to undergo overall deformation, such as arched,[44-46] waved,[47] folded,[48, 49] interlocked,[50-52] microporous,[53, 54] and fibrous.[55]

The overall deformation is more complicated and many of them require higher preparation conditions. With the use of a huge number of spacers and the expansion of the deformation area in the large-area TENG, the above-mentioned shortcomings would become more notable.

Here, we proposed a new type of engraved pattern spacer triboelectric nanogenerator (EPS-TENG) that can harvest energy from mechanical impact. This design just engraves different patterns on the substrate and folds them into evenly distributed small spacers, without introducing additional third-party spacers or deforming the substrate material as a whole. The output of the device under different impact conditions of the motor is systematically investigated. The driving experiment of the timer shows the considerable application prospect of the EPS-TENG in powering portable electronics.

Results and discussion

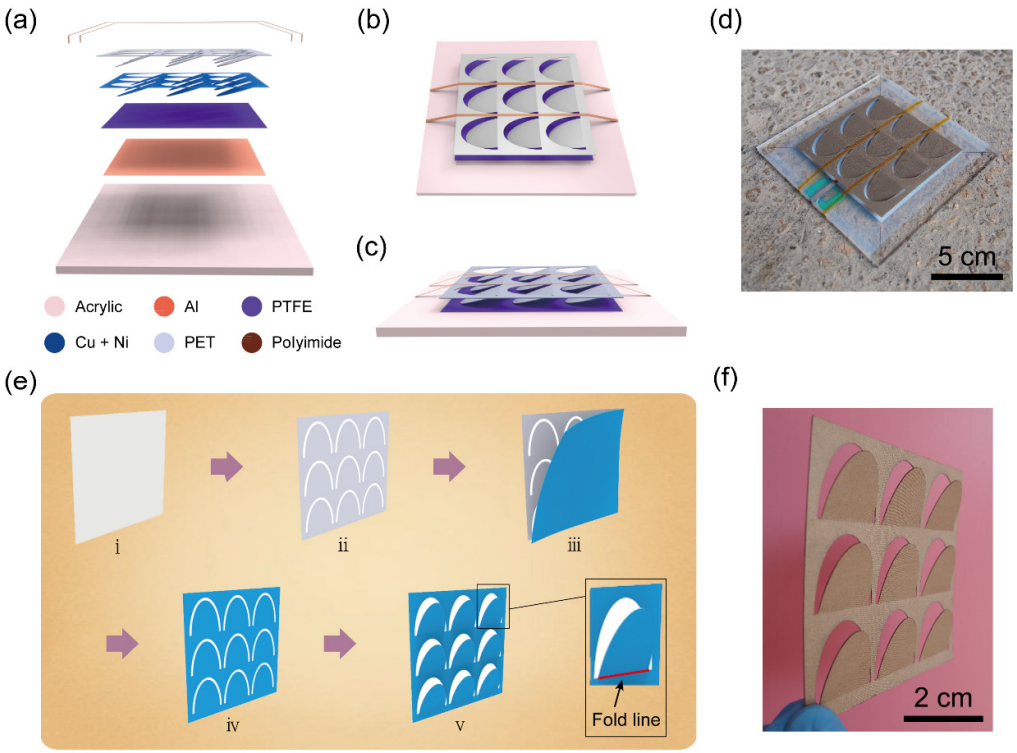

Fig. 1. Structure of the EPS-TENG and preparation process of the engraved pattern spacers. (a)

Exploded view of the device. (b, c) Top and side views of the EPS-TENG, respectively. (d) Photograph of the device. (e) Fabrication procedure of the engraved pattern spacers. Inset: enlarged graph of an engraved pattern spacer showing the location of the fold line. (f) Photograph of the tribometal electrode part with engraved pattern spacers.

The structure diagram of the device is illustrated in Fig. 1a-c. There are two main parts in this design, namely triboelectronegative material part and tribometal electrode part. The triboelectronegative material part is made of a poly(tetrafluoroethylene) (PTFE) film with back Al electrode attached to the acrylic plate. The tribometal electrode part is composed of many folded engraved semi-elliptical spacers, which are evenly distributed on a poly(ethylene terephthalate) (PET) substrate and covered with Cu + Ni cloth of the same shape. The tribometal electrode part is mounted on the triboelectronegative material part vertically and directly opposite, and two thin flexible polyimide tapes are used to tie the above two parts together. It should be emphasized that the polyimide tapes play an important role in preventing the tribometal electrode part from constantly jumping to one side due to the rebound of the semi-elliptical spacers under periodic external impact. From the side view of the EPS-TENG in Fig. 1c, it is obvious that owing to the presence of the folded engraved semi-elliptical spacers, the Cu + Ni cloth and the PTFE film are in an initial state of separation. At the same time, these folded engraved semi-elliptical spacers are all elastic, which is highly desired for the continuous contact and separation between the Cu + Ni cloth and the PTFE film, which will be discussed more later. The microstructure images of the respective surfaces of the Cu + Ni cloth and PTFE film are shown in Fig. S1 (Supporting Information). Fig. 1d is a photograph of the entire prepared EPS-TENG. The specific fabrication process of the engraved pattern spacers is detailed in Fig. 1e. Firstly, some semi-elliptical patterns are engraved on a flat PET substrate, and each semi-elliptical patten has a gap on the periphery of the arc edge to avoid the movement of the semi-elliptical pattern spacers from being disturbed by burrs on the edge. (i-ii). Secondly, the Cu + Ni cloth is covered on the PET substrate (iii). Thirdly, the same semi-elliptical patterns and gaps as the PET substrate are carved on the Cu + Ni cloth (iv). At last, the

engraved semi-elliptical patterns are folded to the side where the Cu + Ni cloth is attached along the fold line, which is the straight edge of the semi-elliptical pattern as shown by the red line in the enlarged inset (v). The entire successfully prepared tribometal electrode part with engraved pattern spacers is shown in Fig. 1f.

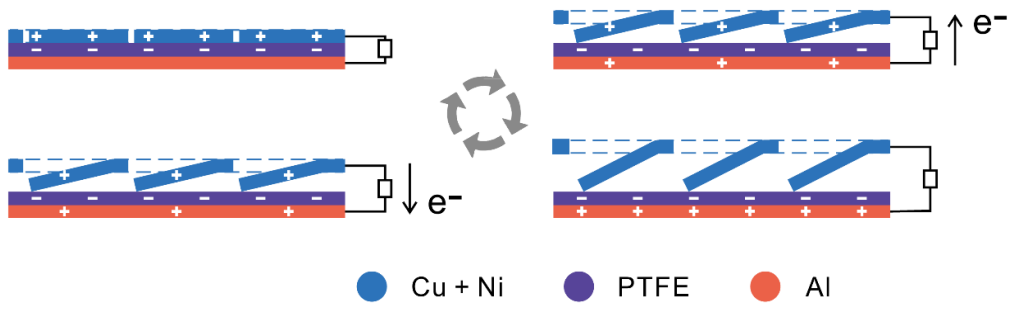

Fig. 2. Schematic sketch of the working principle of the EPS-TENG (not to scale).

Fig. 2 schematically shows the working principle of the EPS-TENG, which is based on the contact-separation mode TENG that couples the contact charging and electrostatic effect.[56, 57] The specific working process of the device is divided into three steps. In the first step, the folding engraved pattern spacers are flattened by the impact force so that the Cu + Ni cloth is completely contacted with the PTFE film. Here, the Cu + Ni cloth is used as both a tribometal material and a conductive electrode. Due to the significant difference in the affinity of the two materials for charges, net positive charges are generated on the surface of the Cu + Ni cloth and equal net negative charges are leaved on the surface of the PTFE film. Meanwhile, the insulation of the PTFE film can make the net negative charges on the PTFE film surface remain for a long time. Secondly, when the external triggering is withdrawn, the engraved pattern spacers return to their original folding state owing to their own elastic force, accompanied by the gradual separation of the Cu + Ni cloth and the PTFE film until the maximum vertical distance is reached. That drives free electrons from Al back electrode of the PTFE film to the Cu + Ni electrode *via* an external circuit to compensate for the potential difference between the two electrodes. Finally, the engraved pattern spacers are pressed again under another external mechanical impact, the Cu + Ni cloth and the

PTFE film are fully bonded again, and free electrons will flow from the Cu + Ni electrode through the external load back to the Al back electrode of the PTFE film. So far, the above three steps of the EPS-TENG have formed a complete and repeatable cycle of generating electrical energy.

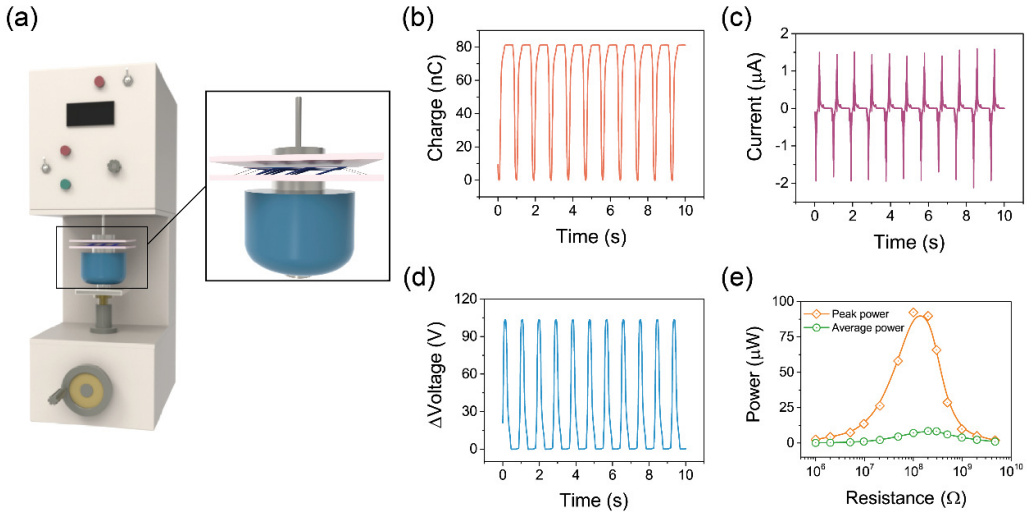

Fig. 3. Basic electrical test of EPS-TENG's output performance. (a) Schematic diagram of the experimental setup. Inset: magnified view of the sensor device installed on the motor. (b-d) Transferred charges (b), short-circuit current (c), and open-circuit voltage (d) of the EPS-TENG. (e) Peak power and average power of the EPS-TENG with different load resistances. The impact force is about 10 N and the impact frequency is 1 Hz.

In order to evaluate the basic output performance of the EPS-TENG, a motor was used in the test, and the impact frequency (f) and force (F) provided by this motor can be adjusted. In the experiment, it is necessary to fix the EPS-TENG on the motor first, and then use a flat acrylic plate as the percussion board to continuously hit the device with the help of the motor. The percussion board has the same size as the acrylic plate that constitutes the EPS-TENG, as shown in Fig. 3a. Here, an EPS-TENG with engraved semi-elliptical pattern spacers are placed on the motor system for testing (the inset in Fig. 3a). Noted that the newly prepared EPS-TENG is not directly used for testing. This is because after more than 100,000 motor shocks ($F < 60$ N and $f \leq 5$ Hz),

the folding degree of the engraved pattern spacers will be irreversibly weakened, but the folding state after weakening to a certain degree is very stable. Then, according to the weakened folding state of the engraved pattern spacers, the polyimide tape was adjusted to obtain a stable structure of the EPS-TENG. Therefore, compared with the newly prepared EPS-TENG, the initial vertical separation height between the Cu + Ni cloth and the PTFE film in the stable structure of the EPS-TENG is smaller and remains at about 5.87 mm. In fact, all the output performance characterizations in our experiments are conducted on the stable structure of the EPS-TENG. Fig. 3b-e shows the outputs of the EPS-TENG with engraved semi-elliptical pattern spacers under an impact with a frequency of 1 Hz and a force of about 10 N. Specifically, the transferred charges are 81.27 nC (Fig. 3b). As an alternator, the EPS-TENG has peak-to-peak short-circuit currents in two directions as shown in Fig. 3c. The positive peak value is 1.6 μA, which corresponds to the separation of the Cu + Ni cloth and the PTFE film after the stress is removed. On the contrary, the other negative peak value is -2.11 μA, belonging to the case where the Cu + Ni cloth is in contact with the PTFE film. The negative sign "-" is only used to identify the direction of the current and has nothing to do with the intensity. The peak-to-peak open-circuit voltage of the device reaches 103.45 V, as shown in Fig. 3d. In addition, we continue to test the peak power and average power of the EPS-TENG, because the peak power and average power of devices with different resistors are intuitive indicators of power generation capacity. The maximum peak power and average power of the EPS-TENG are 92.34 μW and 8.48 μW, and the best matching load resistances are 100.2 MΩ and 199.9 MΩ respectively, as shown in Fig. 3e. The specific corresponding changes in current, voltage, and peak power with load resistance are provided in Fig. S2. The calculation equations for peak power (P_{peak}) and average power (P_{ave}) are as follows:

$$P_{peak} = {I_{peak}}^2 R \tag{1}$$

$$P_{ave} = \frac{\int_0^T I^2 R dt}{T} \tag{2}$$

where I_{peak} is the peak value of the positive current, R is the load resistance, T is 60 s of the output, and I is the output values included both the positive and negative currents.

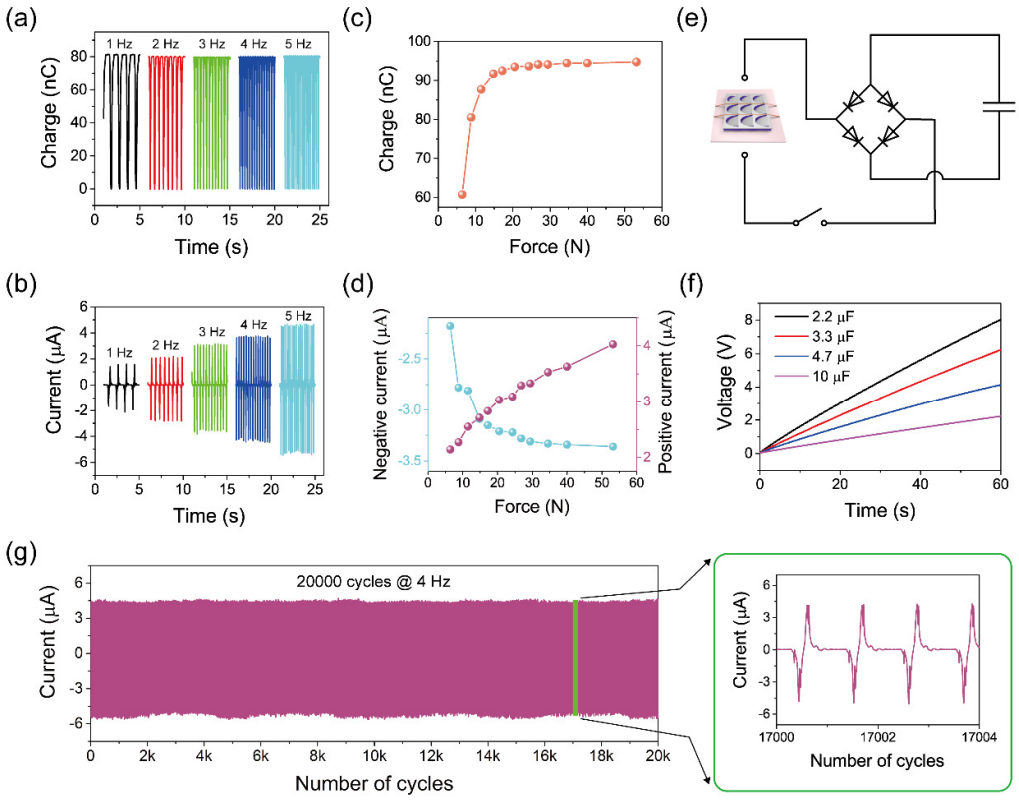

Fig. 4. Output performance of the EPS-TENG. (a, b) Transferred charges (a) and short-circuit current (b) with different impact frequencies. (c, d) Transferred charges (c) and peak short-circuit current (d) with different impact forces. (e) Rectified circuit diagram of the EPS-TENG connected to a capacitor. (f) Charging performance of the EPS-TENG to different capacitors. (g) Stability test of the EPS-TENG reaching 20,000 cycles at a frequency of 4 Hz. Inset: the shot-circuit current waveform of the device in 1 second. The impact force is approximately 10 N and the impact frequency is 2 Hz unless otherwise specified.

We have investigated the device with engraved semi-elliptical spacers in more depth to understand the output performance of the EPS-TENG. The transferred charges and short-circuit current of the EPS-TENG were tested at each integer frequency of 1-5 Hz, as demonstrated in Fig. 4a and b. Under the condition that the impact force is set

to approximately 10 N and the impact frequency is increased sequentially, the transferred charges of the device remain almost unchanged at around 80.2 nC. However, the peak short-circuit current appears to increase linearly, of which 1.6 μA and -2.11 μA, 2.19 μA and -2.81 μA, 3.16 μA and -3.81 μA, 3.77 μA and -4.46 μA, 4.67 μA and -5.44 μA correspond the current output at 1 Hz, 2 Hz, 3 Hz, 4 Hz, and 5 Hz, respectively. This is because the larger the impact frequency, the shorter the time for the same charge transfer, resulting in a proportional increase in the short-circuit current, following the formula $I_{SC} = dQ_{SC}/dt$. Moreover, the influence of different impact forces on the output of the EPS-TENG has been also studied. The premise is to keep the impact frequency at 2 Hz while increasing the impact force. At the beginning, as the force continues to increase, the transferred charges increase quickly, but when the impact force exceeds 20.5 N, the charge output entered a slow-increasing plateau, and the maximum transferred charges of 94.72 nC can be achieved (Fig. 4c). The trend of the transferred charges indicated that the increasing impact force can improve the contact state between the Cu + Ni cloth and the PTFE film in the EPS-TENG.[11] The trend of the negative peak short-circuit current generated by the device with force is roughly the same as that of the transferred charges, and it can eventually reach -3.36 μA. However, the peak value of the positive short-circuit current shows a sustained and rapid increase, and the maximum can reach 4.16 μA (Fig. 4d). Such characteristics should be mainly related to the strong compression of the engraved pattern spacers when the impact force is very large, and the air at the striking interface is greatly squeezed out. As a result, the folding engraved pattern spacers are flattened and temporarily adsorbed on the percussion board together with the PET substrate, similar to a suction cup that uses atmospheric pressure difference, so that the Cu + Ni cloth is driven by the percussion board for a certain distance in the early stage of separation. Therefore, the vertical separation area and speed are effectively increased, which means that more charge transfer occurs per unit time, making the positive peak current continuously increase and even surpasses the negative peak current. The characteristic output of the EPS-TENG under different impact conditions confirms that the device is suitable for energy harvesting in various

mechanical motions. It also implies that the EPS-TENG has the potential to be used as an impact force and frequency sensor in addition to being used as an energy harvester. Usually, TENG devices need to be connected with a capacitor to power low-power electrical appliances, aiming to accumulate the output charges in the capacitor with a long period of time. Fig. 4e is a schematic diagram of the rectified circuit used by the EPS-TENG for charging capacitors. As shown in Fig. 4f, we conducted a 60 s charge test for different capacities under a motor impact of around 10 N and 2 Hz. Specifically, the capacitors of 2.2 μF, 3.3 μF, 4.7 μF, and 10 μF are charged to 8.02 V, 6.23 V, 4.14 V, 2.23 V by the EPS-TENG, and 17.64 μC, 20.56 μC, 19.46 μC, 22.3 μC of charges are stored, respectively. The stability of the device is an important parameter worthy of attention. Thus, we conducted up to 20,000 hitting tests with an impact frequency of 4 Hz and an impact force about 10 N. The short-circuit current output of the device has been very stable without obvious attenuation (Fig. 4g), and the triboelectric surfaces of the Cu + Ni cloth and PTFE film are not significantly worn (Fig. S3). This also reflects that the EPS-TENG has a stable structure and can be used in a working environment that requires multiple runs. The inset of Fig. 4g supplies the waveform of the specific current peak within 1 s of the device intercepted in the output of the latter part of the test.

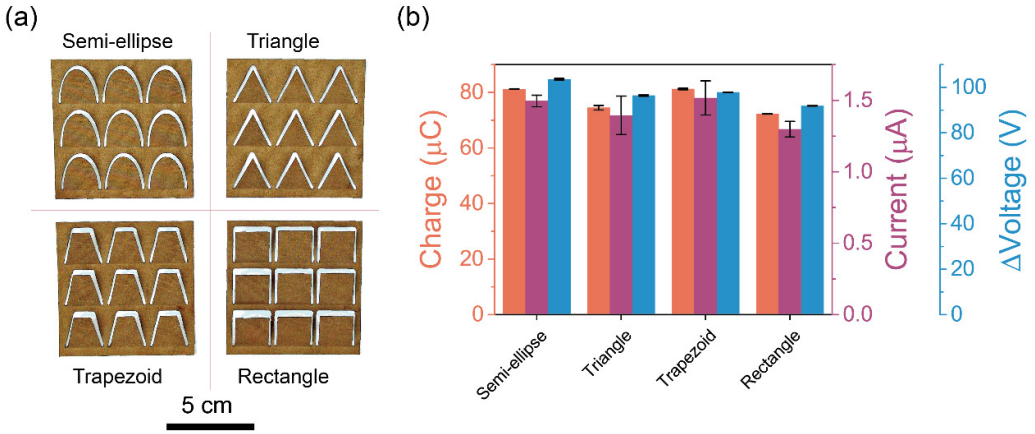

Fig. 5. Output performance of the EPS-TENG with different patterns. (a) Photograph of the EPS-TENG with different patterns. (b) Transferred charges, short-circuit current and open-

circuit voltage of devices with different patterns. The impact force is about 10 N, and the impact frequency is fixed at 1 Hz.

The pattern design of the engraved spacers in the EPS-TENG is versatile, and it was found that engraved spacers with different patterns can also perform the function of elastic spacers, just like the semi-elliptical spacers before. Here, we concisely characterized the electrical performance of the EPS-TENGs with four different engraved patterns, including semi-elliptical, triangular, trapezoidal and rectangular patterns, as shown in Fig. 5a. In this comparative experiment, the impact force of the motor is still about 10 N, and the impact frequency is set at 1 Hz. For the structural design of the EPS-TENG, it is inevitable that different engraved patterns have different gap shapes, and the pattern gap directly affects the area of the Cu + Ni cloth used as the tribometal electrode in the device. However, the largest difference in the gap area of the four patterns is only 219.47 mm^2, which accounts for 3.43% of the total area (i.e. the sum of the Cu + Ni cloth area and the gap area), so the effect of the gap area among these four pattern devices is slight. The measurement results show that the electrical outputs of the EPS-TENGs with different patterns only show ups and downs in a small range (Fig. 5b). Besides the gap area, the factors that cause the output fluctuation should also include the temperature and humidity in the testing environment, the motor impact force, the initial vertical separation height between the Cu + Ni cloth and the PTFE film, the elasticity of the four pattern spacers, etc. From the pattern order of semi-ellipse, triangle, trapezoid to rectangle, the transferred charges of the corresponding devices are 81.22 nC, 74.51 nC, 81.26 nC, 72.25 nC respectively, and the fluctuation range is within 8.97 nC; the positive peak short-circuit currents of these devices are 1.5 μA, 1.4 μA, 1.52 μA, 1.3 μA, and the fluctuation range is within 0.22 μA; the open-circuit voltages of different devices are 103.56 V, 96.4 V, 97.84 V, 91.84 V, and the fluctuation range is 11.72 V. The device outputs with small-scale changes of different engraved patterns can well show that the newly invented EPS-TENG can be used as a prototype, and the feasibility of the pattern is far more than the four examples.

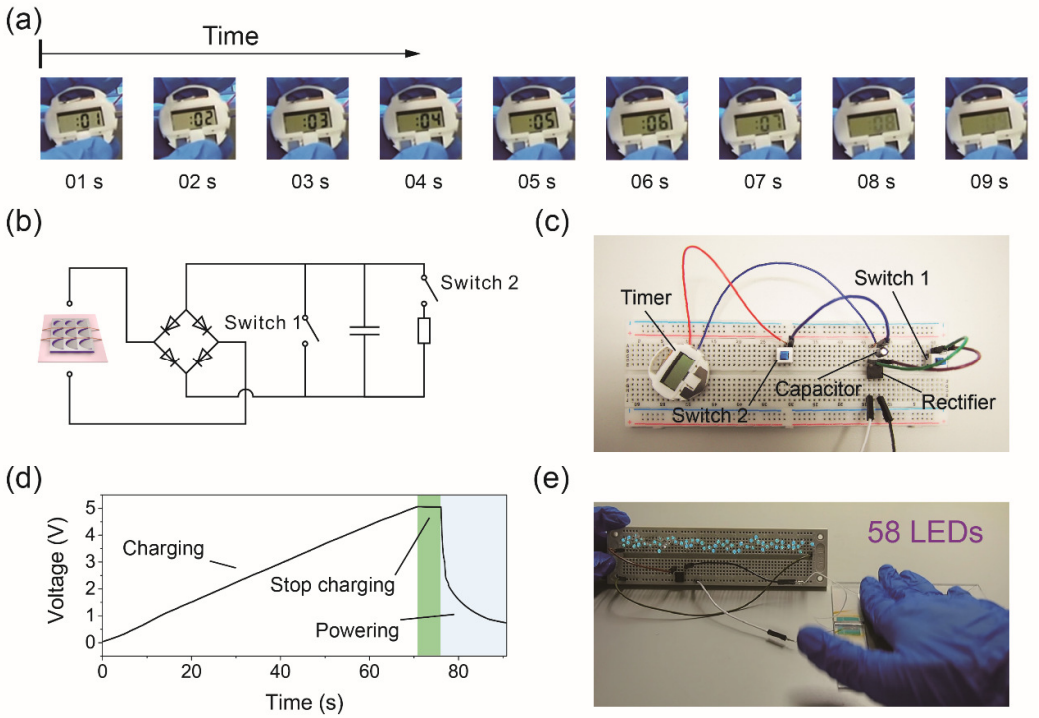

Fig. 6. Demonstration of the EPS-TENG powering electrical loads. (a) Pictures of a timer powered by the EPS-TENG in real time. The time increases from left to right. (b, c) Circuit diagram and photograph of the EPS-TENG for powering the timer. (d) Charging and discharging processes for a capacitor of 10 μF to power the timer. (e) Photograph of the device lighting up 58 LEDs.

The EPS-TENG is a new device with good output performance, and can be used for mechanical energy harvesting. By combining common electrical appliances, we made some intuitive application demonstrations of the EPS-TENG with engraved semi-elliptical spacers under hand tapping. The EPS-TENG can light up 58 LEDs under hand tapping, as presented in Fig. 6e and Video S3. Also, when the device is manually triggered, the LEDs are replaced by a timer as another application combination, which provides a further demonstration of functions. The real-time screen pictures of the timer powered by the EPS-TENG are continuously recorded in Fig. 6a. The pictures show the increment of time from left to right, and the visible timing is 9 s in total. The circuit schematic diagram of the EPS-TENG driving timer is shown in Fig. 6b, and Fig. 6c is the corresponding circuit layout photograph. Specifically, the EPS-TENG is firstly

rectified and connected with a capacitor of 10 μF and an electrical load in parallel. Initially, switch 2 is off and switch 1 is in the on state. Then the switch 1 is turned off, the EPS-TENG relies on hand tapping to complete the 70.65 s charging process for the connected capacitor, and the total stored charges achieve 50.6 μC. Finally, switch 2 is turned on, and the electric energy accumulated in the capacitor is used to power the electrical load, that is, the timer. The corresponding charging and discharging curves of the 10 μF capacitor used for timing demonstration is shown in Fig. 6d, and the operation details are shown in Video S2. Here, the EPS-TENG is proposed as a new prototype featuring engraved pattern spacers, and it is demonstrated that the EPS-TENG can effectively harvest the energy of human movement, such as hand tapping, and use it for driving timer. However, the EPS-TENG is not limited to capturing individual mechanical energy. In the future, it is also expected to contribute to the use of global macro clean energy such as wave energy and wind energy.

Conclusions

In summary, an engraved pattern spacer triboelectric nanogenerator for effectively harvesting mechanical energy is proposed. The engraved pattern spacers in the device are elastic and can be deformed immediately after the impact force is exerted, and can also be automatically restored after the impact force is removed. This ensures the contact and separation of the Cu + Ni cloth and the PTFE film in the device, resulting in that the EPS-TENG can effectively respond to external periodic mechanical shocks. The motor test provides detailed output characteristics of the EPS-TENG under impacts with different frequencies and forces. The output peak power and average power of the device have reached 92.34 μW and 8.48 μW, respectively, and the current output was stable even in 20,000 cycles. In addition, the engraved spacers can be designed with patterns, and the relative device output is well in the test, showing very little fluctuation among them. The driving demonstration of the timer reflects the practical value of the EPS-TENG in energy harvesting. Such excellent performance EPS-TENG can be widely used in environmental mechanical energy harvesting and provides an important

prototype for the design of other engraved spacer devices.

Experimental section

Fabrication of the EPS-TENG. The PET substrate used in the tribometal electrode part is 80 mm × 80 mm × 0.3 mm in length, width, and thickness. A computerized numerical control engraving machine was used to engrave the patterns, and the gaps on the periphery of different patterns are all 1.6 mm wide. The Cu + Ni cloth attached to the PET substrate has a thickness of 0.08 mm. The fold line and fold direction of the triangular, trapezoidal and rectangular patterns are the same as those of the semi-elliptical pattern. The fold line of each pattern is 20 mm long, and the width of each pattern perpendicular to the fold line is also 20 mm. The patterned spacers were manually bent to about 90° along the fold line and fold direction and then loosened. The size of the acrylic plate used for triboelectronegative material part is 120 mm × 120 mm × 3.64 mm in length, width, and thickness. A layer of Al electrode (80 mm × 80 mm × 0.06 mm in length, width, and thickness) was pasted on the top center of the acrylic plate. A PTFE film (0.08 mm in thickness) was covered on the Al electrode. The adhesion between the acrylic plate and the Al electrode, the Al electrode and the PTFE film, the Cu + Ni cloth and the PET substrate was completed by using a pressure-sensitive adhesive. Both the flexible polyimide tapes are 2 mm wide.

Characterization. The transferred charges, current and voltage of the EPS-TENG and the voltage of the capacitor were measured by an electrometer (Keithley 6514). A motor (Fangding ZX-AF02) was used to excite the EPS-TENG, and the impact force of the motor was measured by a dynamometer (Interface 9860-2). When the EPS-TENG was tapped by hand for application demonstration, nitrile gloves were wearing on the hands.

Acknowledgements

The authors would like to acknowledge the funding support from The Hong Kong

Polytechnic University (1-CD43, G-YWA2) for the work reported here.

References

[1] F. R. Fan, Z. Q. Tian, Z. L. Wang, Nano Energy 1 (2012) 328-334.
[2] Z. L. Wang, Materials Today 20 (2017) 74-82.
[3] Y. Zi, H. Guo, Z. Wen, M.-H. Yeh, C. Hu, Z. L. Wang, ACS nano 10 (2016) 4797-4805.
[4] J. Q. Zhao, G. W. Zhen, G. X. Liu, T. Z. Bu, W. B. Liu, X. P. Fu, P. Zhang, C. Zhang, Z. L. Wang, Nano Energy 61 (2019) 111-118.
[5] L. Liu, Q. F. Shi, Z. D. Sun, C. K. Lee, Nano Energy 86 (2021) 106154.
[6] W. Q. Du, J. Nie, Z. H. Ren, T. W. Jiang, L. Xu, S. J. Dong, L. Zheng, X. Y. Chen, H. X. Li, Nano Energy 51 (2018) 260-269.
[7] Z. M. Tian, G. C. Shao, Q. Zhang, Y. N. Geng, X. Chen, Micromachines 10 (2019).
[8] Z. Qin, Y. Y. Yin, W. Z. Zhang, C. J. Li, K. Pan, ACS applied materials & interfaces 11 (2019) 12452-12459.
[9] K. Q. Xia, D. Wu, J. M. Fu, N. A. Hoque, Y. Ye, Z. W. Xu, Journal of Materials Chemistry A 8 (2020) 25995-26003.
[10] F. Xing, Y. Jie, X. Cao, T. Li, N. Wang, Nano Energy 42 (2017) 138-142.
[11] L. Xu, Y. K. Pang, C. Zhang, T. Jiang, X. Y. Chen, J. J. Luo, W. Tang, X. Cao, Z. L. Wang, Nano Energy 31 (2017) 351-358.
[12] T. Jiang, H. Pang, J. An, P. J. Lu, Y. W. Feng, X. Liang, W. Zhong, Z. L. Wang, Advanced Energy Materials 10 (2020) 2000064.
[13] Z. Q. Yuan, C. F. Wang, J. G. Xi, X. Han, J. Li, S. T. Han, W. C. Gao, C. F. Pan, Acs Energy Letters 6 (2021) 2809-2816.
[14] H. Y. Wang, Q. Y. Zhu, Z. Y. Ding, Z. L. Li, H. W. Zheng, J. J. Fu, C. L. Diao, X. A. Zhang, J. J. Tian, Y. L. Zi, Nano Energy 57 (2019) 616-624.
[15] L. Q. Liu, X. Y. Yang, L. L. Zhao, H. X. Hong, H. Cui, J. L. Duan, Q. M. Yang, Q. W. Tang, ACS nano 15 (2021) 9412-9421.
[16] J. S. Lee, H. Yong, Y. I. Choi, J. Ryu, S. Lee, International Journal of Precision Engineering and Manufacturing-Green Technology (2021).
[17] S. W. Xu, Y. G. Feng, Y. Liu, Z. S. Wu, Z. N. Zhang, M. Feng, S. N. Zhang, G. Y. Sun, D. A. Wang, Nano Energy 85 (2021).
[18] X. Chen, X. C. Ma, W. W. Ren, L. X. Gao, S. Lu, D. Q. Tong, F. Y. Wang, Y. Chen, Y. Huang, H. He, B. P. Tang, J. J. Zhang, X. Q. Zhang, X. J. Mu, Y. Yang, Cell Reports Physical Science 1 (2020).
[19] J. X. Zhao, J. L. Mu, H. R. Cui, W. J. He, L. Zhang, J. He, X. Gao, Z. Y. Li, X. J. Hou, X. J. Chou, Advanced Materials Technologies 6 (2021).
[20] Q. Wang, H. X. Zou, L. C. Zhao, M. Li, K. X. Wei, L. P. Huang, W. M. Zhang, Applied Physics Letters 117 (2020).
[21] Q. Zhang, C. M. Jiang, X. J. Li, S. F. Dai, Y. B. Ying, J. F. Ping, ACS nano 15 (2021) 12314-12323.
[22] J. H. Lee, S. Kim, T. Y. Kim, U. Khan, S. W. Kim, Nano Energy 58 (2019) 579-584.
[23] X. Liu, A. F. Yu, A. M. Qin, J. Y. Zhai, Advanced Materials Technologies 4 (2019).

[24] Y. Q. Liu, N. Sun, J. W. Liu, Z. Wen, X. H. Sun, S. T. Lee, B. Q. Sun, ACS nano 12 (2018) 2893-2899.
[25] Q. J. Liang, X. Q. Yan, X. Q. Liao, Y. Zhang, Nano Energy 25 (2016) 18-25.
[26] X. L. Liu, K. Cheng, P. Cui, H. Qi, H. F. Qin, G. Q. Gu, W. Y. Shang, S. J. Wang, G. Cheng, Z. L. Du, Nano Energy 66 (2019).
[27] S. Chatterjee, S. R. Burman, I. Khan, S. Saha, D. Choi, S. Lee, Z. H. Lin, Nanoscale 12 (2020) 17663-17697.
[28] W. Kim, D. Bhatia, H. J. Hwang, K. Choi, D. Choi, Functional Composites and Structures 1 (2019).
[29] C. G. Zhang, L. L. Zhou, P. Cheng, D. Liu, C. L. Zhang, X. Y. Li, S. X. Li, J. Wang, Z. L. Wang, Advanced Energy Materials 11 (2021) 2003616.
[30] X. F. Wang, S. M. Niu, F. Yi, Y. J. Yin, C. L. Hao, K. Dai, Y. Zhang, Z. You, Z. L. Wang, ACS nano 11 (2017) 1728-1735.
[31] L. Jin, W. L. Deng, Y. C. Su, Z. Xu, H. Meng, B. Wang, H. P. Zhang, B. B. Zhang, L. Zhang, X. B. Xiao, M. H. Zhu, W. Q. Yang, Nano Energy 38 (2017) 185-192.
[32] L. M. Zhang, F. Xue, W. M. Du, C. B. Han, C. Zhang, Z. L. Wang, Nano Research 7 (2014) 1215-1223.
[33] Y. J. Su, G. R. Chen, C. X. Chen, Q. C. Gong, G. Z. Xie, M. L. Yao, H. L. Tai, Y. D. Jiang, J. Chen, Advanced materials 33 (2021).
[34] Z. Zhou, X. Li, Y. Wu, H. Zhang, Z. Lin, K. Meng, Z. Lin, Q. He, C. Sun, J. Yang, Z. L. Wang, Nano Energy 53 (2018) 501-507.
[35] Z. F. Zhao, X. Pu, C. H. Du, L. X. Li, C. Y. Jiang, W. G. Hu, Z. L. Wang, ACS nano 10 (2016) 1780-1787.
[36] M. Ha, S. Lim, S. Cho, Y. Lee, S. Na, C. Baig, H. Ko, ACS nano 12 (2018) 3964-3974.
[37] F. Iqbal, M. Shafi, M. I. Khattak, A. Nawaz, Tehnicki Vjesnik-Technical Gazette 25 (2018) 325-328.
[38] S. Wang, Y. Wang, D. H. Liu, Z. Y. Zhang, W. X. Li, C. X. Liu, T. L. Du, X. Xiao, L. G. Song, H. C. Pang, M. Y. Xu, Sensor Actuat a-Phys 317 (2021).
[39] X. A. Shen, W. J. Han, Y. F. Jiang, Q. J. Ding, X. Li, X. Zhao, Z. Y. Li, Energy Reports 6 (2020) 2851-2860.
[40] M. S. Zhu, Y. Huang, W. S. Ng, J. Y. Liu, Z. F. Wang, Z. Y. Wang, H. Hu, C. Y. Zhi, Nano Energy 27 (2016) 439-446.
[41] G. Zhu, Z. H. Lin, Q. S. Jing, P. Bai, C. F. Pan, Y. Yang, Y. S. Zhou, Z. L. Wang, Nano letters 13 (2013) 847-853.
[42] T. C. Hou, Y. Yang, H. L. Zhang, J. Chen, L. J. Chen, Z. L. Wang, Nano Energy 2 (2013) 856-862.
[43] H. M. Zhang, Y. X. Lu, A. Ghaffarinejad, P. Basset, Nano Energy 51 (2018) 10-18.
[44] S. H. Wang, L. Lin, Z. L. Wang, Nano letters 12 (2012) 6339-6346.
[45] W. Tang, B. Meng, H. X. Zhang, Nano Energy 2 (2013) 1164-1171.
[46] Y. L. Chen, Y. C. Wang, Y. Zhang, H. Y. Zou, Z. M. Lin, G. B. Zhang, C. W. Zou, Z. L. Wang, Advanced Energy Materials 8 (2018) 1802159.
[47] X. N. Wen, W. Q. Yang, Q. S. Jing, Z. L. Wang, ACS nano 8 (2014) 7405-7412.
[48] S. B. Gong, B. W. Zhang, J. X. Zhang, Z. L. Wang, K. L. Ren, Advanced Functional Materials 30 (2020) 1908724.

[49] P. Bai, G. Zhu, Z.-H. Lin, Q. Jing, J. Chen, G. Zhang, J. Ma, Z. L. Wang, ACS nano 7 (2013) 3713-3719.
[50] C. S. Wu, X. Wang, L. Lin, H. Y. Guo, Z. L. Wang, ACS nano 10 (2016) 4652-4659.
[51] Y. Kang, B. Wang, S. G. Dai, G. L. Liu, Y. P. Pu, C. G. Hu, ACS applied materials & interfaces 7 (2015) 20469-20476.
[52] W. Q. Yang, J. Chen, G. Zhu, J. Yang, P. Bai, Y. J. Su, Q. S. Jing, X. Cao, Z. L. Wang, ACS nano 7 (2013) 11317-11324.
[53] J. Chun, J. W. Kim, W. S. Jung, C. Y. Kang, S. W. Kim, Z. L. Wang, J. M. Baik, Energy & Environmental Science 8 (2015) 3006-3012.
[54] H. J. Oh, J. H. Bae, Y. K. Park, J. Song, D. K. Kim, W. Lee, M. Kim, K. J. Heo, Y. Kim, S. H. Kim, B. J. Yeang, S. J. Lim, Polymers 12 (2020).
[55] J. W. Zhong, Y. Zhang, Q. Z. Zhong, Q. Y. Hu, B. Hu, Z. L. Wang, J. Zhou, ACS nano 8 (2014) 6273-6280.
[56] S. M. Niu, S. H. Wang, L. Lin, Y. Liu, Y. S. Zhou, Y. F. Hu, Z. L. Wang, Energy & Environmental Science 6 (2013) 3576-3583.
[57] S. M. Niu, Z. L. Wang, Nano Energy 14 (2015) 161-192.